Insights Into the Electric Double-Layer Capacitance of the Two-Dimensional Electrically Conductive Metal-Organic Framework $Cu_3(HHTP)_2$

Jamie W. Gittins[1], Chloe J. Balhatchet[1], Yuan Chen[1, 2, 3], Cheng Liu[4], David G. Madden[5], Sylvia Britto[6], Matthias J. Golomb[7], Aron Walsh[7], David Fairen-Jimenez[5], Siân E. Dutton[4], Alexander C. Forse[1]*

[1] Yusuf Hamied Department of Chemistry, University of Cambridge, Lensfield Road, Cambridge CB2 1EW, U.K.

[2] Department of Chemistry, Imperial College London, Exhibition Road, London SW7 2AZ, U.K.

[3] The Faraday Institution, Quad One, Harwell Science and Innovation Campus, Didcot OX11 0RA, U.K.

[4] Cavendish Laboratory, University of Cambridge, JJ Thomson Avenue, Cambridge CB3 0HE, U.K.

[5] Adsorption & Advanced Materials Laboratory (A^2ML), Department of Chemical Engineering & Biotechnology, University of Cambridge, Philippa Fawcett Drive, Cambridge CB3 0AS, U.K.

[6] Diamond Light Source, Harwell Science and Innovation Campus, Didcot OX11 0DE, U.K.

[7] Department of Materials, Imperial College London, Exhibition Road, London SW7 2AZ, U.K.

Abstract

Two-dimensional electrically conductive metal-organic frameworks (MOFs) are candidate electrode materials for use in electric double-layer capacitor (EDLC) structure-property investigations due to their well-defined crystalline structures. Their promising capacitive performance was first illustrated by EDLCs constructed with the layered framework $Ni_3(HITP)_2$ (HITP = 2,3,6,7,10,11-hexaiminotriphenylene) and an organic electrolyte. Despite this promise, there have been few follow-up studies on the use of these frameworks in EDLCs, raising questions about the generality of the results. Here, we demonstrate the high capacitive performance of the layered framework $Cu_3(HHTP)_2$ (HHTP = 2,3,6,7,10,11-hexahydroxytriphenylene) in EDLCs with an organic electrolyte and compare its performance with $Ni_3(HITP)_2$. $Cu_3(HHTP)_2$ exhibits a specific capacitance of 110 – 114 F g^{-1} at low current densities of 0.04 – 0.05 A g^{-1} and shows modest capacitance retentions (66 %) at current densities up to 2 A g^{-1}, mirroring the performance of $Ni_3(HITP)_2$. However, we also explore the limitations of $Cu_3(HHTP)_2$ in EDLCs, finding a limited cell voltage window of 1.3 V and only moderate capacitance retention over 30,000 cycles. This illustrates that these materials require

further development to improve their EDLC performance, particularly to reach similar cycling performance levels as porous carbons. Despite this, our work underscores the utility of framework materials in EDLCs and suggests that capacitive performance is largely independent of the identity of the metal node and organic linker molecule, instead being dictated by the three-dimensional structure of the framework. These important insights will aid the design of future conductive MOFs for use in EDLCs.

1. Introduction

The improvement of energy storage devices is critical for society to meet increasing energy demands and allow for the integration of renewable energy sources into energy grids[1–3]. Electric double-layer capacitors (EDLCs), a sub-set of supercapacitors, are among the most promising energy storage devices due to their high power densities, which result in rapid charging/discharging times, and excellent cyclability. As a result, EDLCs have potential uses in applications where other energy storage devices are not suitable e.g., in heavy electrical vehicles, storing energy rapidly from intermittent renewable energy sources[3–6]. However, state-of-the-art industrial EDLCs have low energy densities, which impedes their widespread use. Potential performance gains could be achieved by optimising the structure of the electrodes and this may facilitate the use of supercapacitors more widely. Structure-property investigations to determine how performance varies with electrode structure are challenging with traditional EDLCs as many use porous carbons as the electrode material[7,8]. These tend to have poorly defined structures that are difficult to characterise, leading to structure-property investigations with conflicting results[9–14].

Recently, significant work has been done to develop new electrode materials for EDLCs with well-defined structures. One such class of materials is two-dimensional electrically conductive metal-organic frameworks (MOFs)[15]. These materials are generally formed from the square planar coordination of late transition metal M^{2+} nodes by planar conjugated organic linker molecules to form π-d conjugated 2D sheets. These sheets then stack, normally in an eclipsed or near-eclipsed fashion, to form an extended 3D honeycomb structure, creating pores that run through the material (**Fig. 1a**)[16,17]. Conductive MOFs are promising for use as EDLC electrodes as they have high intrinsic conductivities (up to 2500 S cm^{-1}) and porosities (surface areas of 500 – ca. 1400 m^2 g^{-1})[18–20]. Furthermore, the tuneable crystalline structures of conductive MOFs make them interesting materials for use as model electrodes in structure-property

investigations. Despite this promise and much exploration as electrode materials in other energy storage devices, including batteries, few conductive MOFs have been explored in EDLCs, particularly with more commercially relevant organic electrolytes[21–26]. However, a key example is $Ni_3(HITP)_2$ (HITP = 2,3,6,7,10,11-hexaiminotriphenylene), which demonstrated high capacitive behaviour (111 – 116 F g^{-1} at 0.05 A g^{-1}) as the sole electrode material in a symmetric EDLC with 1 M NEt_4BF_4 in acetonitrile electrolyte[27]. The closely related framework $Cu_3(HHTP)_2$ (HHTP = 2,3,6,7,10,11-hexahydroxytriphenylene) was also explored in EDLCs with aqueous and solid-state gel electrolytes, and while nanowire arrays (NWAs) of this MOF exhibited good capacitive performance, electrodes made using $Cu_3(HHTP)_2$ powder exhibited relatively poor capacitive behaviour[28,29]. Here we build on these studies and present a detailed analysis of the electric double-layer capacitance of $Cu_3(HHTP)_2$ in EDLCs with an organic electrolyte. Using a recently published synthesis, as well as traditional electrode film processing methods, we find that $Cu_3(HHTP)_2$ exhibits very similar performance to $Ni_3(HITP)_2$ in terms of capacitance, rate capability, and cycling stability, suggesting that EDLC performance is independent of the identity of the metal node and organic linker in these almost isostructural frameworks[30].

2. Results & Discussion

$Cu_3(HHTP)_2$ was synthesised by modifying a recently published procedure (see SI Methods)[30]. The identity and structure of the MOF were confirmed via powder X-ray diffraction (PXRD), with the experimentally obtained PXRD pattern comparing well to those simulated using eclipsed and near-eclipsed polytypes of the C-centred monoclinic crystal structure of $Cu_3(HHTP)_2$ (**Fig. 1**, SI Figs. S1, S2; Table S1). This supports previous work indicating that $Cu_3(HHTP)_2$ may have a near-eclipsed crystal structure, with a constant stacking shift of the 2D layers of $Cu_3(HHTP)_2$, as opposed to the closely related eclipsed structure exhibited by $Ni_3(HITP)_2$[31]. However, the quality of the PXRD data is insufficient for Rietveld refinement and therefore insufficient to distinguish between the models with any degree of certainty. We subsequently evaluated the porosity and Brunauer, Emmett and Teller (BET) areas using 77 K N_2 adsorption isotherms. A maximum BET area of 794 $m^2\ g^{-1}$ was calculated using Rouquerol's updated criteria implemented in BETSI (SI Fig. S3)[32]. This is the highest reported BET area for this material, comparable to the BET area of $Ni_3(HITP)_2$, and confirms permanent porosity, a key requirement for double-layer capacitance[27,33]. To characterise the Cu oxidation states present in $Cu_3(HHTP)_2$, Cu K-edge X-ray absorption near edge structure (XANES) was performed on a powdered sample. This confirmed that Cu(II) is the dominant Cu oxidation state in the as-synthesised MOF with no clear evidence for the presence of Cu(I) (SI Fig. S4). This result helps to clarify debate in the literature on the Cu oxidation states in the framework, with some previous XANES and X-ray photoelectron spectroscopy (XPS) investigations indicating the presence of Cu(I) in the MOF synthesised using different methods[34,35]. Elemental analysis confirmed that the as-synthesised $Cu_3(HHTP)_2$ has approximately the correct stoichiometric ratio of Cu and HHTP, although a small amount of a N-containing impurity was also present, most likely due to the use of ammonia as a modulator in the synthesis (see SI Methods).

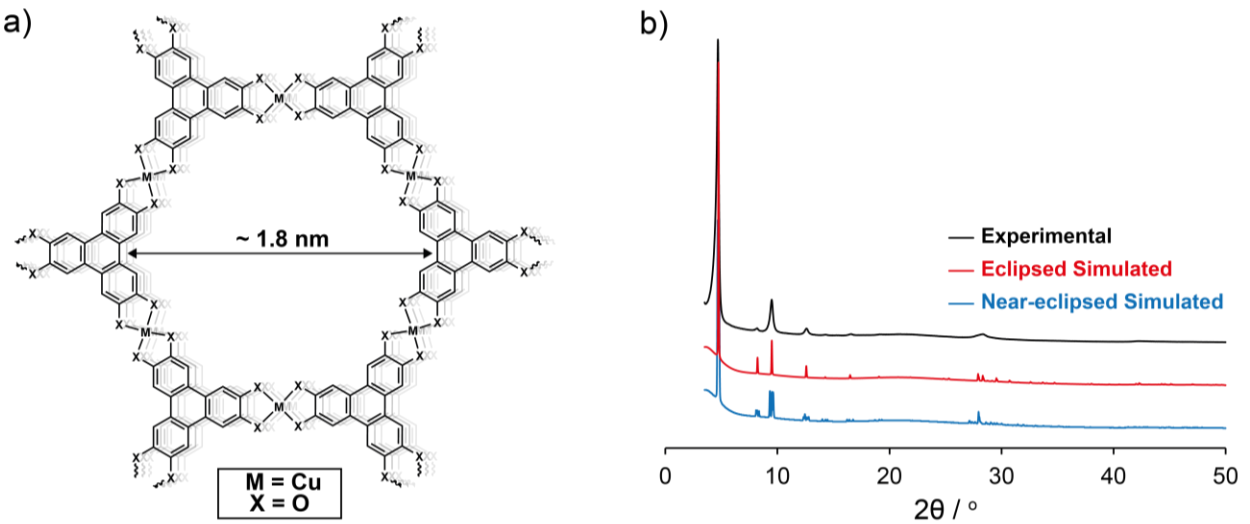

Figure 1: a) Schematic demonstrating the general structure of hexasubstituted triphenylene-based conductive MOFs. The π-d conjugated 2D sheets stack to form an extended 3D honeycomb structure. This creates pores/channels that run through the material, with a pore size of 1.8 nm as calculated from the simulated structure of $Cu_3(HHTP)_2$. b) The experimental PXRD pattern of $Cu_3(HHTP)_2$ compares well to simulated PXRD patterns of $Cu_3(HHTP)_2$ with both eclipsed and near-eclipsed C-centred monoclinic crystal structures (space group = C2/m).

Having characterised the crystalline structure and porosity of $Cu_3(HHTP)_2$, we next examined its electrical conductivity as this is a further key requirement for EDLC electrodes. The electrical conductivity of a pressed pellet of $Cu_3(HHTP)_2$ (two-point probe) was measured as 0.007 S cm^{-1} (see SI Methods). This is comparable to previously reported values for this MOF (0.0001 – 0.3 S cm^{-1} for polycrystalline samples)[21,28,31,36]. Composite films of $Cu_3(HHTP)_2$ (85 wt. % $Cu_3(HHTP)_2$, 10 wt. % carbon black, and 5 wt. % PTFE) of ca. 250 µm thickness were prepared by adapting the traditional literature method for the preparation of activated carbon (AC) films (see SI Methods)[37]. Carbon black was used as a conductive additive to increase the electrical conductivity of the film for use in EDLCs, and has negligible contribution to the total capacitance of the cell (SI Fig. S5). Films made without the conductive additive (95 wt. % $Cu_3(HHTP)_2$ and 5 wt. % PTFE) displayed highly resistive behaviour in EDLCs and required very low current densities for analysis, showing the necessity of the conductive additive to achieve good capacitive performance (SI Figs. S6, S7). This indicates a limitation of using this MOF in EDLCs. Interestingly, Cu K-edge XANES on pristine film samples revealed evidence for the

presence of Cu(I), with the amount of Cu(I) observed varying between samples (SI Fig. S8). Linear combination fitting of this XANES data with standard compounds indicated a maximal Cu(I) content of approximately 20 % (SI Fig. S9; Table S2). This underscores the sensitivity of $Cu_3(HHTP)_2$ and modification of the film-making procedure could be considered in future work if Cu(I) content proves to be problematic.

To investigate the electrochemical double-layer capacitance of $Cu_3(HHTP)_2$, symmetrical EDLCs were assembled using composite $Cu_3(HHTP)_2$ film electrodes and 1 M NEt_4BF_4 in acetonitrile electrolyte (see SI Methods). Cyclic voltammograms (CVs) and galvanostatic charge-discharge (GCD) experiments on these cells showed nearly rectangular and triangular traces respectively (**Fig. 2**), indicative of electrochemical double-layer capacitance. An initial cell voltage window of approximately 1.0 V, where primarily electric double-layer behaviour was observed, was established for $Cu_3(HHTP)_2$ by running CVs with progressively higher final voltages. Beyond 1.0 V, faradaic processes centred at ca. 1.1 V were observed (SI Fig. S10). This stable voltage window was confirmed by running CVs of $Cu_3(HHTP)_2$ composite electrodes in a three-electrode arrangement with 1 M NEt_4BF_4 in acetonitrile. Electric double-layer capacitive behaviour and no faradaic activity were observed for $Cu_3(HHTP)_2$ between the open circuit potential of +0.33 V and –0.27 V vs. Ag in the anodic direction, and between the open circuit potential of +0.19 V and +0.79 V vs. Ag in the cathodic direction (SI Figs. S11, S12). This is consistent with a working voltage window for $Cu_3(HHTP)_2$ EDLCs of approx. 1.0 – 1.2 V, which is further discussed below. This sharply contrasts to traditional activated carbons, which have a larger typical working voltage window of ca. 2.5 V with this electrolyte[38].

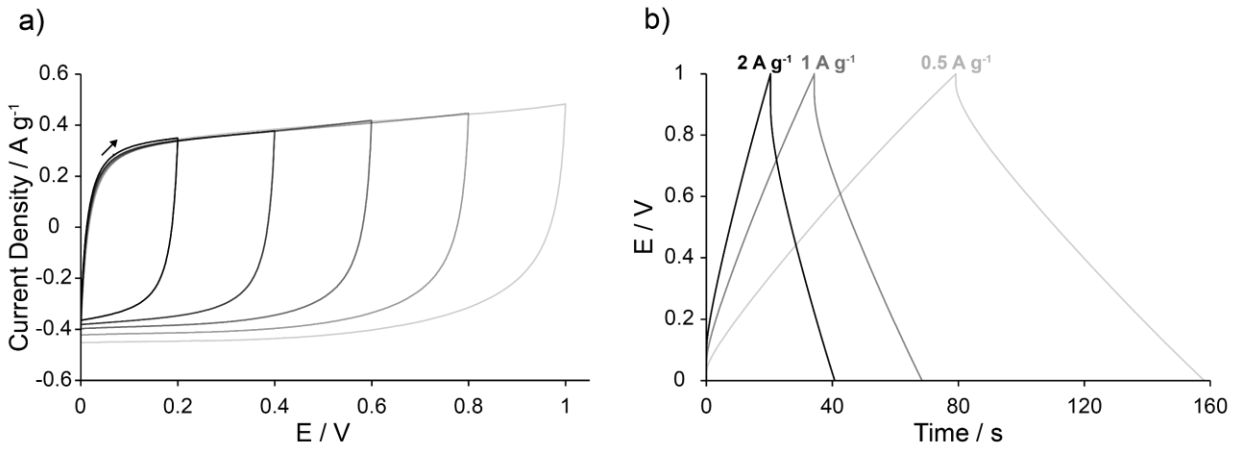

Figure 2: a) Cyclic voltammograms (CVs) at a scan rate of 10 mV s^{-1} up to 1.0 V show that $Cu_3(HHTP)_2$ displays predominantly double-layer capacitive behaviour in this voltage window in symmetric EDLCs with 1 M NEt_4BF_4 in acetonitrile electrolyte. The black arrow shows the direction of scanning from the start of the scan. b) Galvanostatic charge-discharge (GCD) profiles at a variety of current densities confirm this behaviour (see labels).

To evaluate and compare the capacitive performance of $Cu_3(HHTP)_2$ with other electrode materials, specific capacitance (C_g) was calculated at a variety of current densities from GCD profiles using the *Supycap* Python code (see SI Methods). At a low current density of 0.04 – 0.05 A g^{-1}, the specific capacitance of $Cu_3(HHTP)_2$ in EDLCs as assembled above was recorded as 110 – 114 F g^{-1} when charged between 0 – 1 V (SI Fig. S13, Table S3). This value is very similar to that recorded previously for the almost isostructural framework $Ni_3(HITP)_2$ at a similar current density (111 – 116 F g^{-1}) in a similar EDLC with 1 M NEt_4BF_4 in acetonitrile[27]. Increasing the current density leads to a decrease in the specific capacitance (**Fig. 3**), again with very similar results to those reported for $Ni_3(HITP)_2$. Interestingly, these results suggest that the identity of the metal node (Cu or Ni) and ligating heteroatom (O or N) have little/no impact on the double-layer capacitance of these two frameworks. Indeed, $Ni_3(HITP)_2$ and $Cu_3(HHTP)_2$ have very similar 3D structures, with both formed from the eclipsed or near-eclipsed stacking of 2D π-d conjugated layers[18,31,39]. Therefore, our results suggest high capacitive performance arises from the three-dimensional structures of these MOFs. These results further suggest that the capacitance of an EDLC is uniquely defined by the 3D structure of the electrode and the electrolyte used. This generality has not been previously demonstrated using porous carbon materials, although further work is needed to confirm this hypothesis. The equivalent series

resistances (*ESR*s) of the EDLC cells were measured using both electrochemical impedance spectroscopy (EIS) and GCD profiles, with *ESR*s of between 7 – 18 Ω obtained for a range of cells (SI Fig. S14).

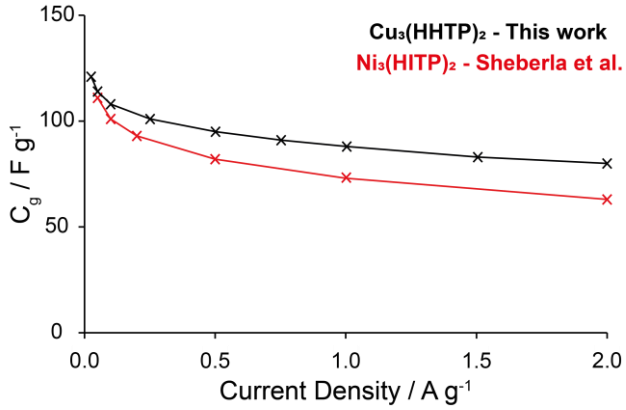

Figure 3: Comparison of specific capacitance versus current density graphs for $Cu_3(HHTP)_2$ and $Ni_3(HITP)_2$ (literature)[27]. This demonstrates the similarity in the capacitance of these MOFs in similar symmetric EDLCs.

Furthermore, we note higher capacitance retention (79 % between 0.25 A g^{-1} – 2 A g^{-1}; 72 % between 0.25 A g^{-1} – 2.5 A g^{-1}) than obtained in previous studies using $Cu_3(HHTP)_2$ powder electrodes in symmetric solid-state EDLCs (30 % up to 2 A g^{-1}), and capacitance retention on par with that obtained with $Cu_3(HHTP)_2$ NWAs in aqueous (58 % up to 2.5 A g^{-1}) and solid-state (60 % up to 2 A g^{-1}) EDLCs[28,29]. Although a direct comparison with solid-state cells is difficult due to the different phases of the electrolytes, these results illustrate that high capacitive behaviour can be achieved using $Cu_3(HHTP)_2$ powder and a conductive additive, which has a simpler synthesis than NWAs (SI Fig. S15). However, it must be noted that higher specific capacitances were observed for devices constructed with NWA electrodes (120 F g^{-1} at 0.5 A g^{-1} with a solid-state electrolyte; 195 F g^{-1} at 0.5 A g^{-1} with aqueous electrolyte) than observed in this work[28,29].

Another common metric used to compare EDLC performance of electrode materials is the areal (surface area normalised) capacitance. In this work, the areal capacitance of $Cu_3(HHTP)_2$ was calculated as approx. 14 μF cm^{-2} at 0.05 A g^{-1}. Although this is lower than that reported for $Ni_3(HITP)_2$ (18 μF cm^{-2}), significant variation in our values between 14 and 23 μF cm^{-2} was observed for EDLCs prepared using independent samples of $Cu_3(HHTP)_2$ with different BET surface areas (SI Table S4). We also observed variations in the performances of assembled EDLCs as a function of the areal mass loading of the electrodes. In general, EDLCs with higher areal mass loadings exhibited a more rapid decrease in capacitance as a function of current density and a higher *ESR* than those with lower areal mass loadings (SI Fig. S13, Table S3). This is consistent with previous observations but highlights the need for clear communication on mass loadings when comparing electrode performances[27,40].

To further investigate the suitability of $Cu_3(HHTP)_2$ for both practical supercapacitor applications and structure-property investigations, the voltage limits and cycling stability were studied in more detail. To probe the voltage limits of the cell, GCD experiments at a current density of 0.1 A g^{-1} were run with increasing final cell voltages from 0.6 V until the failure of the cell was observed. This showed an initial consistent increase in the specific capacitance with increasing final voltage followed by a rapid decrease upon cycling beyond 1.3 V (**Fig. 4a**). This demonstrates that the voltage limit of $Cu_3(HHTP)_2$ in a symmetric EDLC is approximately 1.3 V under these charging/discharging conditions, beyond which rapid degradation of the $Cu_3(HHTP)_2$ electrodes occurs causing irreversible loss in capacitance. Rapid capacitance loss when cycling above this cell voltage was confirmed via CV experiments cycling up to cell voltages of 1.6 V (SI Fig. S16). Degradation was confirmed by examining the Cu K-edge XANES of $Cu_3(HHTP)_2$ composite electrodes from an EDLC held at a cell voltage of 1.5 V for 1 h (SI Fig. S17). A shift of the absorption edge to a lower energy, in addition to the appearance of an inflection at ca. 8981 eV, indicate formation of Cu(I) in the negative electrode. In the

positive electrode, the appearance of the feature at ca. 8981 eV indicates a significant change in the coordination environment around Cu to a lower symmetry environment. The shift of the rising edge to higher energies suggests an oxidation process may occur in the positive electrode too. These results indicate fundamental changes to the MOF structure in both electrodes and hint at potential degradation mechanisms, although further work is required to study these processes in more detail.

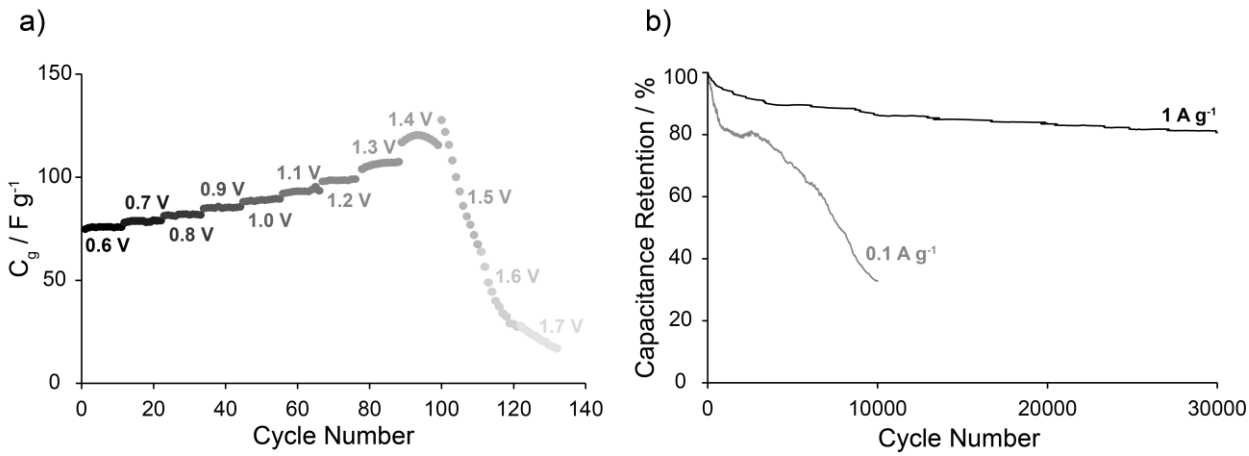

Figure 4: a) Specific capacitance, calculated from GCD profiles, against cycle number for increasing final cell voltages (see labels). This illustrates the voltage limit of the symmetric $Cu_3(HHTP)_2$ EDLC. b) Capacitance retention as a function of cycle number when cycling at 1 A g^{-1} and 0.1 A g^{-1} up to 1.0 V.

To further explore the working voltage window of $Cu_3(HHTP)_2$ EDLCs, Cu K-edge XANES studies were carried out on electrodes extracted from EDLCs held at different cell voltages for a period of 1 h (SI Fig. S18). For a cell voltage of 0.5 V, minimal changes were observed in the XANES spectra. However, for a cell voltage of 0.8 V, the XANES data suggest structural changes to $Cu_3(HHTP)_2$ in the positive electrode. This suggests that kinetically slow faradaic processes may occur at cell voltages below 1.1 V but are missed due to the scan rates used in the above electrochemistry experiments (**Fig. 2**). This hypothesis was confirmed by obtaining a CV at a scan rate of 0.1 mV s^{-1} up to 1 V, with faradaic activity observed at this slow scan rate upon cycling past 0.8 V (SI Fig. S19). This highlights that $Cu_3(HHTP)_2$ may only be kinetically stable up to 1 V, a possible limitation that is explored further below.

Finally, the cycling stability of symmetric $Cu_3(HHTP)_2$ EDLCs was investigated at two different current densities in GCD experiments limited to a maximum cell voltage of 1 V. Reasonable cycling stability was observed when cycled between 0 – 1 V at 1 A g^{-1}, with capacitance retention of 81 % over 30,000 cycles (**Fig. 4b**). The capacitance retentions after 5,000 and 10,000 cycles (90 % and 86 %, respectively) compare well with the retentions of $Ni_3(HITP)_2$, approx. 90% over 10,000 cycles, and $Cu_3(HHTP)_2$ NWA devices with an aqueous electrolyte, 79.9 % over 5,000 cycles (SI Figs. S20, S21)[27,29]. This further highlights the similarities in electrochemical performance between $Ni_3(HITP)_2$ and $Cu_3(HHTP)_2$, and is further evidence that electrodes manufactured from $Cu_3(HHTP)_2$ powder can achieve high EDLC performance on par with those made with $Cu_3(HHTP)_2$ NWAs. Cu K-edge XANES showed minimal changes to the edge position and pre-edge peaks following this cycling, confirming the stability of $Cu_3(HHTP)_2$ upon extensive cycling at this current density (SI Fig. S22).

However, the capacitance retention of $Cu_3(HHTP)_2$ is significantly lower than that of YP50F, a commercial microporous AC, when cycled in an EDLC with 1 M NEt_4BF_4 in acetonitrile. In our work, YP50F exhibited a capacitance retention of 99 % over 10,000 cycles when cycled between 0 – 2.5 V at 2 A g^{-1} (SI Figs. S23, S24). This illustrates that, while this family of MOFs have specific and areal capacitances on par or exceeding current state-of-the-art carbons, significant improvement is required to achieve comparable cycling stability. This is the first work to call attention to this key difference and illustrates a major disadvantage of using this family of conductive MOFs in EDLCs instead of ACs, as high cycling stability is a crucial property of an EDLC. Furthermore, the capacitance retention of $Cu_3(HHTP)_2$ EDLCs in this work was significantly lower when cycled at a lower current density of 0.1 A g^{-1}, with only 32 % capacitance retention after 10,000 cycles (**Fig. 4b**). An increase in the intensity of the pre-edge feature at ca. 8981 eV was observed in the Cu K-edge XANES of the positive electrode following cycling, again indicative of a change in the MOF structure. A shift in the absorption

edge energy to a lower value was also seen, hinting at possible Cu(I) formation. This confirms degradation at this current density (SI Fig. S25) and further emphasises that $Cu_3(HHTP)_2$ is only kinetically stable when cycled between 0 – 1 V. This is also the first work to highlight the difference in capacitance retention at different current densities with this family of conducting frameworks. These findings raise questions about the practical applicability of these frameworks in commercial devices. Future studies to identify the degradation mechanisms in these frameworks may allow for the design of conductive MOFs with wider double-layer stability windows, and thus improved capacitive performances. Given the observation of redox processes centred on the Cu nodes by XANES, varying the metal node may be a viable method to increase the potential window[41].

3. Conclusion

In summary, we have demonstrated that the conductive MOF $Cu_3(HHTP)_2$ displays good capacitive behaviour in symmetric EDLCs with 1 M NEt_4BF_4 in acetonitrile, with a specific capacitance of 110 – 114 F g^{-1} at 0.04 – 0.05 A g^{-1} recorded. Our work shows that the previously observed capacitive behaviour of $Ni_3(HITP)_2$ is not unique amongst layered conducting MOFs, and has expanded the family of conductive MOFs which is known to display capacitive performance in EDLCs with organic electrolytes. Notably, $Cu_3(HHTP)_2$ can be synthesised using all commercially available starting materials, and we have demonstrated that standard electrode fabrication techniques using $Cu_3(HHTP)_2$ powder can be employed with this framework to achieve good capacitive performance, making this framework an accessible model system for further study. However, our work also illustrates a number of limitations of using current conductive MOFs in EDLCs, notably the significantly lower cycling stability and stable double-layer voltage window relative to state-of-the-art carbon materials. This raises questions about the practical applicability of these frameworks in commercial devices. Despite this, the similarity in the specific capacitances of $Cu_3(HHTP)_2$ and $Ni_3(HITP)_2$ at low current densities with the same organic electrolyte shows that the capacitive performance is independent of the identity of the metal node and organic linker molecule for these two frameworks. Importantly, this suggests that the capacitive performance of an EDLC more generally is uniquely defined by the 3D structure of the electrodes and the electrolyte, although further work is required to test this significant hypothesis.

Associated content

Supporting Information

The Supplementary Information (SI) is available free of charge.

Details of experimental procedures, PXRD analysis, gas sorption analysis, additional electrochemistry data and analysis, and additional XANES data and analysis (PDF)

Author Information

Corresponding Author

*Email: acf50@cam.ac.uk

Notes

The authors declare no competing financial interest.

Acknowledgments

J.W.G. acknowledges the School of the Physical Sciences (Cambridge) for the award of an Oppenheimer Studentship. This work was supported by the Faraday Institution [grant number FIRG017], via a Faraday Undergraduate Summer Experience (FUSE) internship to Y.C. The work at Imperial (A.W.) was supported by a Royal Society University Research Fellowship (UF100278) and benefited from the UK Materials and Molecular Modelling Hub for computational resources, which is partially funded by EPSRC (EP/P020194/1 and EP/T022213/1). M.J.G. thanks the Royal Society of Chemistry for PhD funding. D.F.-J. thanks the European Research Council (ERC) under the European Union's Horizon 2020 Research and Innovation Programme (NanoMOFdeli), ERC-2016-COG 726380, and Innovate UK (104384). S.E.D. acknowledges funding from the Winton Programme for the Physics of Sustainability (Cambridge). A.C.F. thanks the Isaac Newton Trust of Trinity College (Cambridge) for a Research Grant, and the Department of Chemistry (Cambridge) for the award of a BP Next Generation Fellowship. This work was also supported by a UKRI Future Leaders Fellowship to A.C.F. (MR/T043024/1). We thank the Diamond Light Source for the award of beam time as part of the Energy Materials Block Allocation Group SP14239. We thank Dr. Phillip Milner and Dr.

Lewis Owen for collaboration and stimulating discussion over the course of the project. We thank Dr. Chris Truscott and Dr. Nigel Howard for collaboration and technical expertise.

References

(1) World Energy Outlook 2019. *World Energy Outlook; OECD* **2019**. https://doi.org/10.1787/caf32f3b-en.

(2) al Shaqsi, A. Z.; Sopian, K.; Al-Hinai, A. Review of Energy Storage Services, Applications, Limitations, and Benefits. *Energy Reports* **2020**, 288–306. https://doi.org/10.1016/j.egyr.2020.07.028.

(3) Gü, T. M. Review of Electrical Energy Storage Technologies, Materials and Systems: Challenges and Prospects for Large-Scale Grid Storage. *Energy & Environmental Science* **2018**, *11*, 2696. https://doi.org/10.1039/c8ee01419a.

(4) González, A.; Goikolea, E.; Barrena, J. A.; Mysyk, R. Review on Supercapacitors: Technologies and Materials. *Renewable and Sustainable Energy Reviews* **2016**, 1189–1206. https://doi.org/10.1016/j.rser.2015.12.249.

(5) Simon, P.; Gogotsi, Y.; Dunn, B. Where Do Batteries End and Supercapacitors Begin? *Science* **2014**, *343* (6176), 1210–1211. https://doi.org/10.1126/science.1248080.

(6) Liu, X.; Li, K. Energy Storage Devices in Electrified Railway Systems: A Review. *Transportation Safety and Environment* **2020**, *2* (3), 183–201. https://doi.org/10.1093/tse/tdaa016.

(7) Miller, E. E.; Hua, Y.; Tezel, F. H. Materials for Energy Storage: Review of Electrode Materials and Methods of Increasing Capacitance for Supercapacitors. *Journal of Energy Storage* **2018**, 30–40. https://doi.org/10.1016/j.est.2018.08.009.

(8) Méndez-Morales, T.; Ganfoud, N.; Li, Z.; Haefele, M.; Rotenberg, B.; Salanne, M. Performance of Microporous Carbon Electrodes for Supercapacitors: Comparing Graphene with Disordered Materials. *Energy Storage Materials* **2019**, *17*, 88–92. https://doi.org/10.1016/j.ensm.2018.11.022.

(9) Chmiola, J.; Yushin, G.; Dash, R.; Gogotsi, Y. Effect of Pore Size and Surface Area of Carbide Derived Carbons on Specific Capacitance. *Journal of Power Sources* **2006**, *158* (1), 765–772. https://doi.org/10.1016/j.jpowsour.2005.09.008.

(10) Largeot, C.; Portet, C.; Chmiola, J.; Taberna, P. L.; Gogotsi, Y.; Simon, P. Relation between the Ion Size and Pore Size for an Electric Double-Layer Capacitor. *Journal of the American Chemical Society* **2008**, *130* (9), 2730–2731. https://doi.org/10.1021/ja7106178.

(11) Chmiola, J.; Yushin, G.; Gogotsi, Y.; Portet, C.; Simon, P.; Taberna, P. L. Anomalous Increase in Carbon at Pore Sizes Less than 1 Nanometer. *Science* **2006**, *313* (5794), 1760–1763. https://doi.org/10.1126/science.1132195.

(12) Centeno, T. A.; Sereda, O.; Stoeckli, F. Capacitance in Carbon Pores of 0.7 to 15 Nm: A Regular Pattern. *Physical Chemistry Chemical Physics* **2011**, *13* (27), 12403–12406. https://doi.org/10.1039/c1cp20748b.

(13) Stoeckli, F.; Centeno, T. A. Optimization of the Characterization of Porous Carbons for Supercapacitors. *Journal of Materials Chemistry A* **2013**, *1*, 6865–6873. https://doi.org/10.1039/c3ta10906b.

(14) Raymundo-Piñero, E.; Kierzek, K.; Machnikowski, J.; Béguin, F. Relationship between the Nanoporous Texture of Activated Carbons and Their Capacitance Properties in Different Electrolytes. *Carbon* **2006**, *44* (12), 2498–2507. https://doi.org/10.1016/j.carbon.2006.05.022.

(15) Liu, J.; Song, X.; Zhang, T.; Liu, S.; Wen, H.; Chen, L. 2D Conductive Metal–Organic Frameworks: An Emerging Platform for Electrochemical Energy Storage. *Angewandte Chemie - International Edition* **2020**. https://doi.org/10.1002/anie.202006102.

(16) Xie, L. S.; Skorupskii, G.; Dincă, M. Electrically Conductive Metal-Organic Frameworks. *Chemical Reviews* **2020**, 8536–8580. https://doi.org/10.1021/acs.chemrev.9b00766.

(17) Hmadeh, M.; Lu, Z.; Liu, Z.; Gándara, F.; Furukawa, H.; Wan, S.; Augustyn, V.; Chang, R.; Liao, L.; Zhou, F.; Perre, E.; Ozolins, V.; Suenaga, K.; Duan, X.; Dunn, B.; Yamamto, Y.; Terasaki, O.; Yaghi, O. M. New Porous Crystals of Extended Metal-Catecholates. *Chemistry of Materials* **2012**, *24* (18), 3511–3513. https://doi.org/10.1021/cm301194a.

(18) Ko, M.; Mendecki, L.; Mirica, K. A. Conductive Two-Dimensional Metal-Organic Frameworks as Multifunctional Materials. *Chemical Communications* **2018**, *54*, 7873. https://doi.org/10.1039/c8cc02871k.

(19) Sun, L.; Campbell, M. G.; Dincə, M. Electrically Conductive Porous Metal-Organic Frameworks. *Angewandte Chemie - International Edition* **2016**, 3566–3579. https://doi.org/10.1002/anie.201506219.

(20) Dou, J.-H.; Arguilla, M. Q.; Luo, Y.; Li, J.; Zhang, W.; Sun, L.; Mancuso, J. L.; Yang, L.; Chen, T.; Parent, L. R.; Skorupskii, G.; Libretto, N. J.; Sun, C.; Yang, M. C.; Dip, P. V.; Brignole, E. J.; Miller, J. T.; Kong, J.; Hendon, C. H.; Sun, J.; Dincă, M. Atomically Precise Single-Crystal Structures of Electrically Conducting 2D Metal–Organic Frameworks. *Nature Materials* **2020**. https://doi.org/10.1038/s41563-020-00847-7.

(21) Nam, K. W.; Park, S. S.; dos Reis, R.; Dravid, V. P.; Kim, H.; Mirkin, C. A.; Stoddart, J. F. Conductive 2D Metal-Organic Framework for High-Performance Cathodes in Aqueous Rechargeable Zinc Batteries. *Nature Communications* **2019**, *10* (1). https://doi.org/10.1038/s41467-019-12857-4.

(22) Feng, D.; Lei, T.; Lukatskaya, M. R.; Park, J.; Huang, Z.; Lee, M.; Shaw, L.; Chen, S.; Yakovenko, A. A.; Kulkarni, A.; Xiao, J.; Fredrickson, K.; Tok, J. B.; Zou, X.; Cui, Y.; Bao, Z. Robust and Conductive Two-Dimensional Metal− Organic Frameworks with Exceptionally High Volumetric and Areal Capacitance. *Nature Energy* **2018**, *3*, 30–36. https://doi.org/10.1038/s41560-017-0044-5.

(23) Gu, S.; Bai, Z.; Majumder, S.; Huang, B.; Chen, G. Conductive Metal–Organic Framework with Redox Metal Center as Cathode for High Rate Performance Lithium Ion Battery. *Journal of Power Sources* **2019**, *429*, 22–29. https://doi.org/10.1016/j.jpowsour.2019.04.087.

(24) Cai, D.; Lu, M.; Li, L.; Cao, J.; Chen, D.; Tu, H.; Li, J.; Han, W. A Highly Conductive MOF of Graphene Analogue Ni3(HITP)2 as a Sulfur Host for High-Performance Lithium–Sulfur Batteries. *Small* **2019**, *15* (44). https://doi.org/10.1002/smll.201902605.

(25) Li, F.; Zhang, X.; Liu, X.; Zhao, M. Novel Conductive Metal-Organic Framework for a High-Performance Lithium-Sulfur Battery Host: 2D Cu-Benzenehexathial (BHT). *ACS Applied Materials and Interfaces* **2018**, *10* (17), 15012–15020. https://doi.org/10.1021/acsami.8b00942.

(26) Dong, S.; Wu, L.; Xue, M.; Li, Z.; Xiao, D.; Xu, C.; Shen, L.; Zhang, X. Conductive Metal–Organic Framework for High Energy Sodium-Ion Hybrid Capacitors. *ACS Applied Energy Materials* **2021**. https://doi.org/10.1021/acsaem.0c02758.

(27) Sheberla, D.; Bachman, J. C.; Elias, J. S.; Sun, C. J.; Shao-Horn, Y.; Dincă, M. Conductive MOF Electrodes for Stable Supercapacitors with High Areal Capacitance. *Nature Materials* **2017**, *16* (2), 220–224. https://doi.org/10.1038/nmat4766.

(28) Li, W. H.; Ding, K.; Tian, H. R.; Yao, M. S.; Nath, B.; Deng, W. H.; Wang, Y.; Xu, G. Conductive Metal–Organic Framework Nanowire Array Electrodes for High-Performance Solid-State Supercapacitors. *Advanced Functional Materials* **2017**, *27* (27). https://doi.org/10.1002/adfm.201702067.

(29) Du, X.; Zhang, J.; Wang, H.; Huang, Z.; Guo, A.; Zhao, L.; Niu, Y.; Li, X.; Wu, B.; Liu, Y. Solid-Solid Interface Growth of Conductive Metal-Organic Framework Nanowire Arrays and Their Supercapacitor Application. *Materials Chemistry Frontiers* **2020**, *4* (1), 243–251. https://doi.org/10.1039/c9qm00527g.

(30) Hoppe, B.; Hindricks, K. D. J.; Warwas, D. P.; Schulze, H. A.; Mohmeyer, A.; Pinkvos, T. J.; Zailskas, S.; Krey, M. R.; Belke, C.; König, S.; Fröba, M.; Haug, R. J.; Behrens, P. Graphene-like Metal-Organic Frameworks: Morphology Control, Optimization of Thin Film Electrical Conductivity and Fast Sensing Applications. *CrystEngComm* **2018**, *20* (41), 6458–6471. https://doi.org/10.1039/c8ce01264d.

(31) Day, R. W.; Bediako, D. K.; Rezaee, M.; Parent, L. R.; Skorupskii, G.; Arguilla, M. Q.; Hendon, C. H.; Stassen, I.; Gianneschi, N. C.; Kim, P.; Dincă, M. Single Crystals of Electrically Conductive Two-Dimensional Metal-Organic Frameworks: Structural and Electrical Transport Properties. *ACS Central Science* **2019**, *5* (12), 1959–1964. https://doi.org/10.1021/acscentsci.9b01006.

(32) Osterrieth, J. W. M.; Rampersad, J.; Madden, D.; Rampal, N.; Skoric, L.; Connolly, B.; Allendorf, M. D.; Stavila, V.; Snider, J. L.; Ameloot, R.; Marreiros, J.; Ania, C.; Azevedo, D.; Vilarrasa-Garcia, E.; Santos, B. F.; Bu, X.-H.; Zang, X.; Bunzen, H.; Champness, N. R.; Griffin, S. L.; Chen, B.; Lin, R.-B.; Coasne, B.; Cohen, S.; Moreton, J. C.; Colon, Y. J.; Chen, L.; Clowes, R.; Coudert, F.-X.; Cui, Y.; Hou, B.; D, D. M.; Doheny, P. W.; Dincă, M.; Sun, C.; Doonan, C.; Thomas Huxley, M.; Evans, J. D.; Falcaro, P.; Ricco, R.; Farha, O.; Idrees, K. B.; Islamoglu, T.; Feng, P.; Yang, H.; Forgan, R. S.; Bara, D.; Furukawa, S.; Sanchez, E.; Gascon, J.; Telalovic, S.; Ghosh, S. K.; Mukherjee, S.; Hill, M. R.; Munir Sadiq, M.; Horcajada, P.; Salcedo-Abraira, P.; Kaneko, K.; Kukobat, R.; Kenvin, J.; Keskin, S.; Kitagawa, S.; Otake, K.; Lively, R. P.; A DeWitt, S. J.; Llewellyn, P.; Lotsch, B. v; Emmerling, S. T.; Pütz, A. M.; Martí-Gastaldo, C.; Padial, N. M.; García-Martínez, J.;

Linares, N.; Maspoch, D.; Suárez del Pino, J. A.; Moghadam, P.; Oktavian, R.; Morris, R. E.; Wheatley, P. S.; Navarro, J.; Petit, C.; Danaci, D.; Rosseinsky, M. J.; Katsoulidis, A. P.; Schröder, M.; Han, X.; Yang, S.; van der Veen, M. A.; Rega, D.; van Speybroeck, V.; J Rogge, S. M.; Lamaire, A.; Walton, K. S.; Bingel, L. W.; Wuttke, S.; Andreo, J.; Yaghi, O.; Zhang, B.; Yavuz, C. T.; Nguyen, T. S.; Zamora, F.; Montoro, C.; Zhou, H.; Kirchon, A.; Fairen-Jimenez, D. How Reproducible Are Surface Areas Calculated from the BET Equation? *Nature Materials* **2021**, [Manuscript Under Review].

(33) Bi, S.; Banda, H.; Chen, M.; Niu, L.; Chen, M.; Wu, T.; Wang, J.; Wang, R.; Feng, J.; Chen, T.; Dincă, M.; Kornyshev, A. A.; Feng, G. Molecular Understanding of Charge Storage and Charging Dynamics in Supercapacitors with MOF Electrodes and Ionic Liquid Electrolytes. *Nature Materials* **2020**, *19* (5), 552–558. https://doi.org/10.1038/s41563-019-0598-7.

(34) Misumi, Y.; Yamaguchi, A.; Zhang, Z.; Matsushita, T.; Wada, N.; Tsuchiizu, M.; Awaga, K. Quantum Spin Liquid State in a Two-Dimensional Semiconductive Metal-Organic Framework. *Journal of the American Chemical Society* **2020**, *142* (39), 16513–16517. https://doi.org/10.1021/jacs.0c05472.

(35) Mendecki, L.; Mirica, K. A. Conductive Metal-Organic Frameworks as Ion-to-Electron Transducers in Potentiometric Sensors. *ACS Applied Materials and Interfaces* **2018**, *10* (22), 19248–19257. https://doi.org/10.1021/acsami.8b03956.

(36) Rubio-Giménez, V.; Galbiati, M.; Castells-Gil, J.; Almora-Barrios, N.; Navarro-Sánchez, J.; Escorcia-Ariza, G.; Mattera, M.; Arnold, T.; Rawle, J.; Tatay, S.; Coronado, E.; Martí-Gastaldo, C. Bottom-Up Fabrication of Semiconductive Metal–Organic Framework Ultrathin Films. *Advanced Materials* **2018**, *30* (10). https://doi.org/10.1002/adma.201704291.

(37) Dyatkin, B.; Presser, V.; Heon, M.; Lukatskaya, M. R.; Beidaghi, M.; Gogotsi, Y. Development of a Green Supercapacitor Composed Entirely of Environmentally Friendly Materials. *ChemSusChem* **2013**, *6* (12), 2269–2280. https://doi.org/10.1002/cssc.201300852.

(38) Eguchi, T.; Tashima, D.; Fukuma, M.; Kumagai, S. Activated Carbon Derived from Japanese Distilled Liquor Waste: Application as the Electrode Active Material of Electric Double-Layer Capacitors. *Journal of Cleaner Production* **2020**, *259*. https://doi.org/10.1016/j.jclepro.2020.120822.

(39) Chen, T.; Dou, J. H.; Yang, L.; Sun, C.; Libretto, N. J.; Skorupskii, G.; Miller, J. T.; Dincă, M. Continuous Electrical Conductivity Variation in M3(Hexaiminotriphenylene)2(M = Co, Ni, Cu) MOF Alloys. *Journal of the American Chemical Society* **2020**, *142* (28), 12367–12373. https://doi.org/10.1021/jacs.0c04458.

(40) Bhattacharjya, D.; Carriazo, D.; Ajuria, J.; Villaverde, A. Study of Electrode Processing and Cell Assembly for the Optimized Performance of Supercapacitor in Pouch Cell Configuration. *Journal of Power Sources* **2019**, *439*, 227106. https://doi.org/10.1016/j.jpowsour.2019.227106.

(41) Iqbal, R.; Sultan, M. Q.; Hussain, S.; Hamza, M.; Tariq, A.; Akbar, M. B.; Ma, Y.; Zhi, L. The Different Roles of Cobalt and Manganese in Metal-Organic Frameworks for

Supercapacitors. *Advanced Materials Technologies* **2021**, 2000941. https://doi.org/10.1002/admt.202000941.